D. DITTERT
for the HADES Collaboration

Institut für Kernphysik, Technische Universiät Darmstadt
(Darmstadt, Germany; e-mail: d.dittert@gsi.de)

ELECTROMAGNETIC RADIATION FROM Au + Au COLLISIONS AT $\sqrt{s_{NN}} = 2.4$ GeV MEASURED WITH HADES

We present results of low-mass dielectron measurements from Au + Au collisions at $\sqrt{s_{NN}} = 2.4$ GeV with HADES. The focus lies on the extraction of the effective temperature from the differential dilepton spectra and the analysis of the azimuthal anisotropy of virtual photons.

K e y w o r d s: HADES, dielectrons, effective temperature, azimuthal anisotropy.

1. Introduction

The matter created in heavy-ion collisions at relativistic energies is rather compressed than heated, reaching net baryon densities of a few times normal nuclear matter density and moderate temperatures below 70 MeV/k_B. Such matter is commonly described as the resonance matter consisting of a gas of nucleons and excited baryonic states, as well as contributions from mesonic excitations. Due to the compression in the inital phase of the collision, the hadron properties are substantialy modified. To understand the microscopic structure of baryon-dominated matter, HADES systematically measures virtual photons, that decay into dileptons, from elementary and heavy-ion collisions. These electromagnetic probes access the entire space-time evolution of a fireball and leave the collision zone without further interactions. Moreover, in contrast to real photons, they carry an additional information through their invariant mass. Thus, they provide the unique information about the various stages of the collision.

In Au + Au at $\sqrt{s_{NN}} = 2.4$ GeV, HADES observed a strong excess radiation which is remarkably well described assuming the emission out of a thermalized system [1]. Thus, the results imply strong medium effects beyond a pure superposition of individual nucleon-nucleon (*pp*, *np*) collisions.

The total yield of dileptons in the low-mass region up to 1 GeV/c^2 is related to the fireball lifetime [2]. The inverse slope of the invariant mass spectra provides information about the temperature in the system averaged over the whole space-time evolution of the collision [3, 4]. To gain a further insight, the dependence of those temperatures on the virtual photon transverse momentum and rapidity and on the event centrality can be studied. Furthermore, the shapes of the spectra can be confronted with model calculations to obtain the understanding of the processes occurring in low-energy heavy-ion collisions such as the establishment of a local thermal equilibrium and the restoration of the chiral symmetry at high densities leading to modifications in the low-mass in-medium vector meson spectral function [2,5–8]. Using a coarse-grained transport calculation to describe the fireball evolution leads to a good agreement with the experimental data in the region $M_{ee} > 0.3$ GeV/c^2 [9, 10].

This approach implies a locally equilibrated system for which the corresponding thermodynamic parameters can be extracted [2]. However, non-equilibrated transport-calculations also describe the data points without significant deviations.

In addition, the observables related to the collectivity of a system, e.g., the flow, are used to describe the macroscopic properties of nuclear matter. The collective flow consists of a radial flow, which affects the thermal spectra of the outgoing particles, and anisotropic flow, which affects the spatial orientation of the particle momenta. The azimuthal anisotropy is especially useful to disentangle early and late emis-

sion sources, because the effective temperature results from the superposition of all fireball stages with decreasing the temperature T, but increasing the flow β_T over time (see Eq. 4). The azimuthal anisotropies, on the other hand, are actually small in the early phases of the fireball evolution, where the flow is not yet fully developed and grow larger for the later phases. Thus, the elliptic flow does not show this implicit time dependence, and the combined dependence of the elliptic flow of dileptons on their transverse momentum and their invariant mass provides a rich landscape of structures, which allows one to set the observational window on specific stages of the fireball evolution [11].

2. Data Analysis and Signal Extraction

HADES at SIS18 (GSI, Darmstadt, Germany) is a fixed-target experiment. The spectrometer provides a large acceptance between 18° and 85° in the polar angle, as well as a nearly full azimuthal coverage. Figure 1 shows a 3D view of HADES with the main components of the detector. The Ring Imaging CHerenkov detector (RICH), the Time of Flight (TOF) and RPC detector, as well as the Pre-Shower detector, are mainly used for the particle identification, while four planes of low-mass MDCs in combination with a superconducting toroidal magnet are used to determine the particle tracks and momenta. In order to reduce the background from the photon conversion in a detector material, all tracking detectors are designed as light as possible. About 7 m behind the spectrometer, the Forward Wall is placed. It is used to reconstruct the event plane and to determine the centrality of a collision by measuring the spectator nucleons.

In twelve runs between 2002 and 2019, HADES collected data from various experiments at beam energies of 1–3.5 GeV. The size of the collision system ranged from elementary $p + p$ collisions over light- $(C + C)$ and medium-sized $(Ar + KCl)$ collision systems to the large $Au + Au$ system. In the two runs performed in 2014, also the pion-induced reactions were investigated. Before the most recent run $(Ag + Ag @ \sqrt{s_{NN}} = 2.55$ GeV completed in March 2019), the major detector upgrades including the RICH detector and a new electromagnetic calorimeter were conducted. In this work, the results of analysis of the data taken from the $Au + Au$ run at
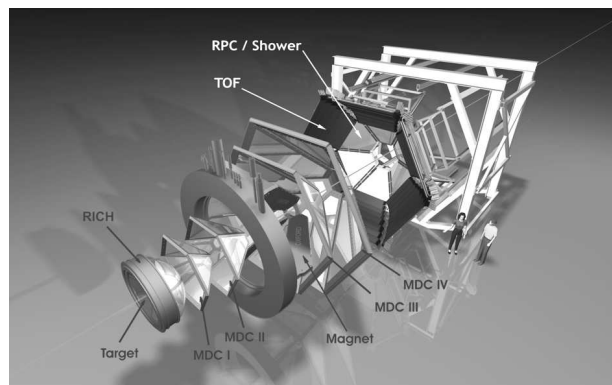

Fig. 1. 3D view of the HADES setup

2.4 GeV [1] in 2012 will be presented. In the five-week beamtime (overall 557 hours) with beam intensities between 1.2–1.5×10^6 ions/s, the total of 7.3 billion events were collected and stored in 138 TB of data [13, 14].

After choosing only the events with a reaction vertex inside the target, rejecting the pile-up events and using a high-multiplicity trigger that selects 47% of the most central events along with event quality selection criteria, a clean sample of about 2.6×10^9 events were left to analyze.

Dileptons are very rare due to low branching ratios, e.g., $\Gamma_{ee}/\Gamma = (4.72 \pm 0.05) \times 10^{-5}$ in the case of a ρ-meson [15]. Thus, a very precise particle identification is crucial for reliable measurements. To separate the leptons from the hadronic background, the hard cuts in one or two dimensions can be applied on various observables. However, a better performance can be achieved, by considering the correlations between all the observables simultaneously, i.e., by using Multivariate Analysis (MVA) methods. They allowed us to identify single leptons with a very high purity of at least 98% and a good efficiency. In order to take the step from the reconstructed single electron signal to the dilepton spectra, the electron-positron pairs have to be build. It is not possible to identify electrons and protons from the same vertex. Instead, all possible unlike-sign pair combinations are calculated event-by-event (Fig. 2, black circles). This leads to a large contribution of wrong pair-

---

[1] A center-of-mass energy of $\sqrt{s_{NN}} = 2.42$ GeV corresponds to a beam energy of $E_{\text{beam}} = 1.23A$ GeV and a center-of-mass rapidity of $y_{\text{mid}} = 0.74$.
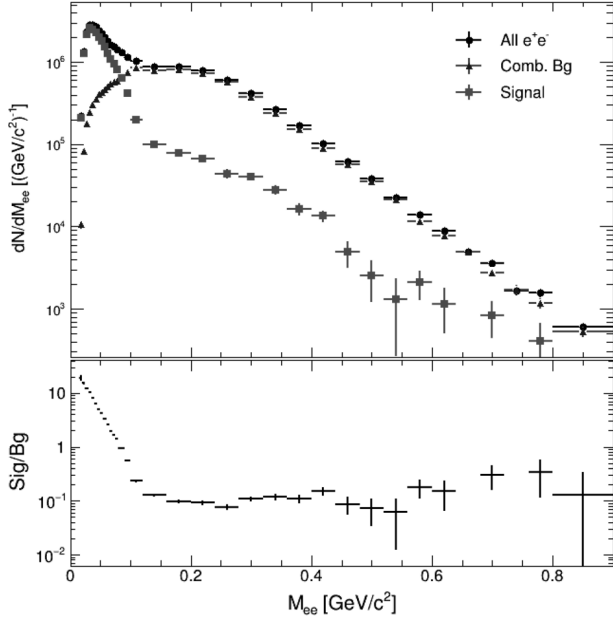
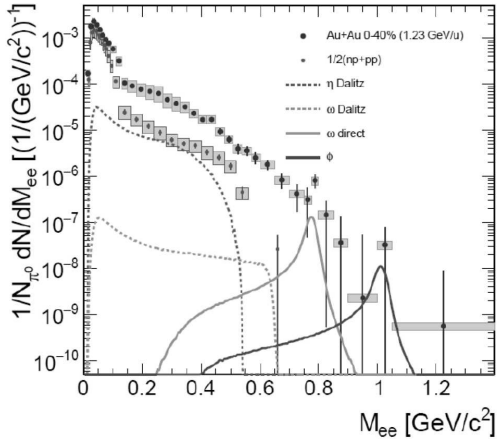**Fig. 2.** Resulting dilepton spectrum and signal-to-background ratio

Fig. 3. Efficiency corrected dilepton spectrum is shown alongside a simulated cocktail of contributions from first chance collisions and the freeze-out stage [17]

ings to the final spectra. This so-called combinatorial background has to be subtracted from all pairs to obtain the true signal pairs (Fig. 2, blue triangles). As usual, two types of fake lepton pairs are distinguished, namely, the uncorrelated and correlated backgrounds. The former one stems from the pairing of leptons, originating from different mother particles, which is the largest contribution to the com-

binatorial background. Due to the random combination of two different decays, it is structureless. In the case of a two-photon decay or a Dalitz decay with the subsequent photon conversion of a neutral meson, it can happen that the paired leptons have different mother particles, but share their grandparent. The correlation of these pairs leads to a background contribution with a bump-like structure. While the uncorrelated background can be reproduced using the event mixing, the correlated background, which is dominant in the low-mass region, is handled using a same-event like-sign technique. The signal is a result of subtracting the combinatorial background from all e^+e^- combinations (Fig. 2, red squares). The signal-to-background ratio (bottom panel of Fig. 2) is $\sim 10\%$ for the invariant masses above 0.15 GeV/c^2.

3. Anisotropy Analysis

The flow coefficients v_1 (directed flow), v_2 (elliptic flow), v_3 (triangular flow), *etc.* are defined as the Fourier coefficients of the azimuthal angle expansion [16]:

$$\frac{dN}{d\Delta\Phi} \propto 1 + 2\sum_{n=1}^{\infty} v_n \cos\left(n\Delta\Phi\right), \quad \Delta\Phi = \Phi_{ee} - \Psi_{\mathrm{EP}}.$$
(1)

To extract the $\Delta\Phi$ of dileptons, the difference of the azimuthal angle of the dilepton pair (Φ_{ee}) and the angle of the event plane (Ψ_{EP}), which is determined using the information of the spectator hits in the Forward Wall, is calculated. This subtraction is necessary due to the correlation between the directed and elliptic flow components and the collision geometry. Furthermore, a correction factor accounting for the event plane angle resolution has to be applied [18]. The anisotropy coefficient v_2^{sig} of the signal pairs is then calculated from [19]:

$$v_2^{\mathrm{sig}} = \frac{1}{r}v_2^{\mathrm{tot}} - \frac{1-r}{r}v_2^{\mathrm{bg}},$$
(2)

where r is the mass-dependent signal-to-background ratio, and v_2^{sig}, v_2^{tot}, and v_2^{bg} represent the flow coefficients for the signal pairs, all pairs, and the combinatorial background pairs. The latter ones are determined using different methods, namely, the same-event like-sign geometric mean background, mixed-event unlike-sign background and making an assumption that the combinatorial pairs, being built

from the same single particles as signal pairs, have also the same orientation with respect to the reaction plane. To obtain a final value for the azimuthal anisotropy, the mean of the different methods is calculated. Their standard deviation is used to determine the systematic uncertainty. The statistical uncertainties are taken from the same-event like-sign geometric mean background for the lowest mass region, where the correlated background from π^0-Dalitz decays is dominant, and from the mixed-event background in the mass regions above.

4. Results

Figure 4 shows the effective slope parameter T_{slope} as a function of the invariant mass of the dielectron pairs, resulting from the fit:

$$\frac{1}{p_T}\frac{dN}{dp_T} \propto m_T K_1\left(\frac{m_T c^2}{k_{\text{B}} T_{\text{slope}}}\right), \tag{3}$$

with $m_T = \sqrt{M_{ee}^2 + p_T^2 c^2}$ and the assumption of a pure Boltzmann nature of the source. Since only a small fraction of the dilepton yield is lying outside of the HADES acceptance, which can be verified by comparing the rapidity spectra to different model calculations, this assumption is justified and is valid to apply a thermal fit without prior extrapolation to the unmeasured rapidity. Utilizing the good agreement between the shapes of the model fits and the experimental p_T spectra, a parametrization of the slopes from the model provides a further quantitative information. From

$$k_{\text{B}} T_{\text{slope}} = k_{\text{B}} T_{\text{kin}} + \frac{1}{2} M_{ee} c^2 \langle\beta_T\rangle^2, \tag{4}$$

where T_{kin} and $\langle\beta_T\rangle$ in the case of dileptons can be interpreted as the properties of their source averaged over four-volume, rather than of the freeze-out hypersurface, the values $T_{\text{kin}} = 65$ MeV/k_{B}, $\langle\beta_T\rangle = 0.19$ for the coarse-grained (CG) approach plus cocktail and $T_{\text{kin}} = 74$ MeV/k_{B}, $\langle\beta_T\rangle = 0.05$ for Hadron String Dynamics (HSD) can be extracted. Extrapolating those model fits to the zero invariant mass results in $T_{\text{min}} = 61$ MeV/k_{B} and $T_{\text{min}} = 69$ MeV/k_{B}, respectively. However, more precise experimental data are needed to decide for one model or another one. Contrary to hadrons [22, 23], the slope parameter is not dependent on the invariant mass, but stays rather constant over the whole mass
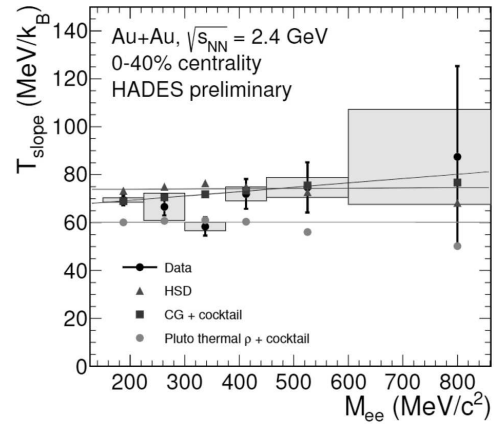

Fig. 4. Fitted slope parameters of the p_T-spectra in experimental data and model calculations of HSD [20], freeze-out meson cocktail combined with the in-medium ρ-spectral function [2] (denoted as CG), and the same cocktail combined with simple thermal ρ simulated using the Pluto event generator [21]. Solid curves represent the parametrization in Eq. 4, fitted to the model points [24]
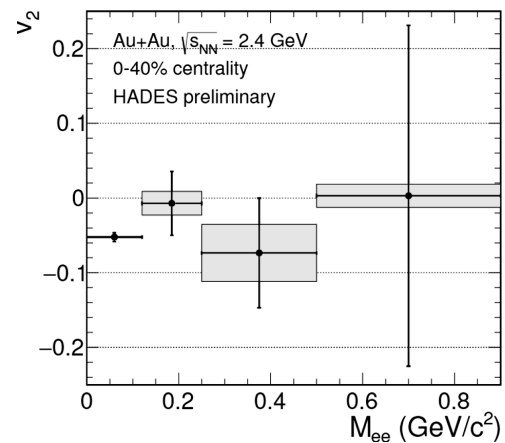

Fig. 5. v_2 coefficient of signal dileptons as a function of the invariant mass [24]

range. This is due to the very low transverse velocity $\langle\beta_T\rangle$, indicating that the majority of dileptons is emitted at an early phase, thus not carrying the full $\langle\beta_T\rangle$ established at the freeze-out.

The second Fourier harmonic of the azimuthal anisotropy as a function of the invariant mass is shown in Fig. 5. The value in the lowest mass region $\left(0 \leq M_{ee}\ [\text{GeV}/c^2] \leq 0.12\right)$, where the dilepton spectrum is dominated by π^0-Dalitz decays, is in a good agreement with the elliptic flow seen in charged pions (see Fig. 6). A negative sign of v_2
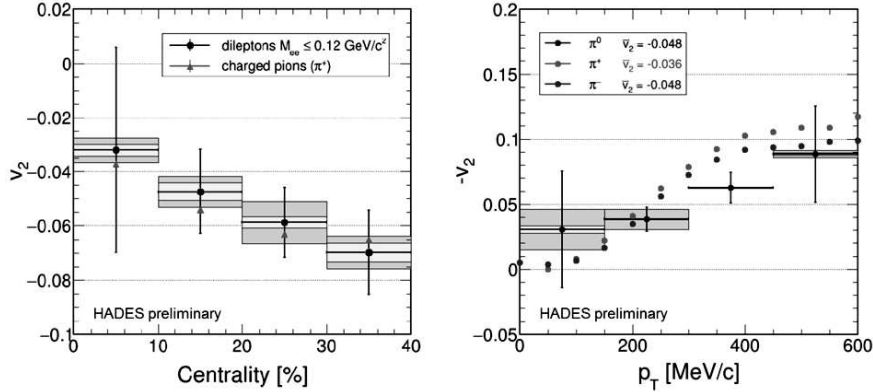
Fig. 6. v_2 of dileptons below 0.12 GeV/c^2 and charged pions as functions of the centrality and transverse momentum

means that the majority of the particles is ejected perpendicularly to the event plane. This out-of-plane flow can be explained by the passing spectator nuclei shadowing the collision center. This shadowing effect reduces the mean free path of particles that are emitted into the reaction plane, which leads to a squeeze-out of ejectiles perpendicularly to the reaction plane. At masses above the π^0-region, the azimuthal anisotropy seems to decrease and indeed is consistent with zero. Recalling the cocktail contributions shown in Fig. 3, it becomes apparent that the physics background contribution in those mass regions is at the level of at most 10% from η-decays, thus much lower than the 90% pion contribution in the first mass bin, meaning that those dileptons are mostly stemming from an early phase before the build-up of the flow. This is consistent with the observed very low transverse velocity discussed above. An alternative explanation of the vanishing azimuthal anisotropy is given by the penetrating nature of dileptons, which therefore do not experience the shadowing effect of the spectator matter [25]. More insights will be provided with the new set of data collected in March 2019, and that data are awaiting for theory interpretations. Figure 6 shows a comparison between v_2 of dileptons below 0.12 GeV/c^2 and charged pions. In the left panel, the centrality-dependent elliptic flow is plotted. As the collision gets more peripheral, more spectator nucleons are shielding the collision zone resulting in a stronger, i.e. more negative, flow. The values from the dileptons from π^0-decays and the charged pions are in a very good agreement. The same is true for

the transverse-momentum-dependent flow coefficients shown in the right panel.

5. Conclusions

The results from the dilepton analysis in Au + Au collisions at 2.4 GeV show a clear evidence for the penetrating nature of the electromagnetic probes. The very low transverse velocity indicates that the majority of dileptons is ejected before the freeze-out, where the full transverse velocity seen in hadrons would have build up. The same is true for the creation of a flow in the system. Thus, the dileptons, which do not stem from hadronic decays show little or no azimuthal anisotropy. However, both methods would profit from higher statistics, as it is not possible up to now to definitely rule out one of the models with the inverse slope analysis or extract the azimuthal anisotropy with higher precision. In the most recent HADES beamtime with Ag + Ag at $\sqrt{s_{NN}} = 2.55$ GeV, conducted in March 2019, $\sim$15 billion events were collected, and the first low-level analysis promises high statistics and a very good data quality. Moreover, a newly installed electromagnetic calorimeter allows one to directly detect neutral mesons, making it possible to further determine the physics background in the dilepton spectra. In addition, the effects of the system size can be investigated. Combining the presented Au + Au data with the recently measured Ag + Ag run, as well as Ar + KCl at $\sqrt{s_{NN}} = 2.6$ GeV, will help one to draw a more complete picture.

1. J. Adamczewski-Musch *et al.* for the HADES Collaboration. Probing dense baryon-rich matter with virtual photons. *Nature Physics* (2019) [DOI: https://doi.org/10.1038/s41567-019-0583-8].

2. T. Galatyuk, P. Hohler, R. Rapp, F. Seck, J. Stroth. Thermal dileptons from coarse-grained transport as fireball probes at SIS energies. *Eur. Phys. J. A* **52**, 131 (2016).

3. H. Specht. Thermal dileptons from hot and dense strongly interacting matter. *AIP Conf. Proceed.* **1322**, 1 (2010).

4. R. Rapp, H. van Hees. Thermal dileptons as fireball thermometer and chronometer. *Phys. Lett. B* **753**, 586 (2016).

5. R. Rapp, J. Wambach, H. van Hees. The chiral restoration transition of QCD and low mass dileptons. *Landolt-Bornstein* **23**, 134 (2010).

6. S. Endres, H. van Hees, J. Weil, M. Bleicher. Dilepton production and reaction dynamics in heavy-ion collisions at SIS energies from coarse-grained transport simulations. *Phys. Rev. C* **92**, 014911 (2015).

7. S. Endres, H. van Hees, J. Weil, M. Bleicher. Coarse-graining approach for dilepton production at energies available at the CERN Super Proton Synchrotron. *Phys. Rev. C* **91**, 054911 (2015).

8. J. Staudenmaier, J. Weil, V. Steinberg, S. Endres, H. Petersen. Dilepton production and resonance properties within a new hadronic transport approach in the context of the GSI-HADES experimental data. *Phys. Rev. C* **98** (5), 054908 (2018).

9. S. Harabasz, (HADES Collaboration). Exploring barion rich matter with heavy-ion collisions. *Ukr. Phys. J.* **64**, 563 (2019).

10. F. Seck, T. Galatyuk, R. Rapp, J. Stroth. Probing the fireball at SIS-18 energies with thermal dilepton radiadtion. *Acta Phys. Polon. Supp.* **10**, 717 (2017).

11. R. Rapp. Dilepton spectroscopy of QCD matter at collider energies. *Adv. High Energy Phys.* **2013**, Article ID 148253 (2013).

12. C. Müntz *et al.* for the HADES-MDC Collaboration. The HADES tracking system. *Nucl. Instrum. Meth. A* **535**, 242 (2004).

13. T. Galatyuk. HADES overview. *Nucl. Phys. A*, **931**, 41 (2014).

14. List of all HADES beamtimes [URL:https://www-hades.gsi.de/?q=node/5].

15. C. Patrignani *et al.* (Particle Data Group). Review of particle physics. *Chinese Phys. C* **40**, 10 (2016).

16. G. Vujanovic, C. Young, B. Schenke, R. Rapp, S. Jeon, C. Gale. Dilepton emission in high-energy heavy-ion collisions with viscous hydrodynamics. *Phys. Rev. C* **89**, 034904 (2014).

17. P. Sellheim. Reconstruction of the low-mass dielectron signal in 1.23A GeV Au + Au collisions. *PhD thesis* (Johann Wolfgang Goethe-Universitet, 2017).

18. J.-Y. Ollitrault. Flow systematics from SIS to SPS energies. *Nucl. Phys. A* **638** (1–2), 195 (1998).

19. L. Adamczyk, *et al.* Dielectron azimuthal anisotropy at mid-rapidity in Au + Au collisions at $\sqrt{s_{NN}}$ = 200 GeV. *Phys. Rev. C* **90**, 064904 (2014).

20. E. Bratkovskaya, J. Aichelin, M. Thomere, S. Vogel, M. Bleicher. System size and energy dependence of dilepton production in heavy-ion collisions at 1–2 GeV/nucleon energies. *Phys. Rev. C* **87**, 064907 (2013).

21. I. Fröhlich, T. Galatyuk, R. Holzmann, J. Markert, B. Ramstein, P. Salabura, J. Stroth. Design of the Pluto event generator. *J. Phys. Conf. Ser.* **219**, 032039 (2010).

22. J. Adamczewski-Musch *et al.* for the HADES Collaboration. Deep sub-threshold Φ production in Au + Au collisions. *Phys. Lett. B* **778**, 403 (2018).

23. J. Adamczewski-Musch *et al.* for the HADES Collaboration. Sub-threshold production of K_s^0 mesons and Λ hyperons in Au + Au collisions at $\sqrt{s_{NN}}$ = 2.4 GeV. *Phys. Lett. B* **793**, 457 (2019).

24. S. Harabasz. Multi-differential pattern of low-mass e^+e^- excess from $\sqrt{s_{NN}}$ = 2.4 GeV Au + Au collisions with HADES. *Nucl. Phys. A* **982**, 771 (2019).

25. A. Wagner *et al.* The emission pattern of high-energy pions: A new probe for the early phase of heavy ion collisions. *Phys. Rev. Lett.* **85** 18 (2000).

Д. Діттерт
від імені Колаборації HADES

ЕЛЕКТРОМАГНІТНЕ ВИПРОМІНЮВАННЯ
В ЗІТКНЕННЯХ Au + Au ПРИ ЕНЕРГІЇ 2,4 ГеВ,
В ДОСЛІДАХ НА HADES

Р е з ю м е

Представляємо результати вимірювання діелектронів малих мас у зіткненнях Au + Au при енергії 2,4 ГеВ у дослідах на HADES з метою отримання ефективної температури з диференційного спектра ділептонів, а також для аналізу азимутальної анізотропії віртуальних фотонів.